H-NeRF: Neural Radiance Fields for Rendering and Temporal Reconstruction of Humans in Motion

Hongyi Xu
Google Research
hongyixu@google.com

Thiemo Alldieck
Google Research
alldieck@google.com

Cristian Sminchisescu
Google Research
sminchisescu@google.com

Abstract

We present H-NeRF, neural radiance fields for rendering and temporal (4D) reconstruction of a human in motion as captured by a sparse set of cameras or even from a monocular video. Our NeRF-inspired approach combines ideas from neural scene representation, novel-view synthesis, and implicit statistical geometric human representations. H-NeRF allows to accurately synthesize images of the observed subject under novel camera views and human poses. Instead of learning a radiance field in empty space, we attach it to a structured implicit human body model, represented using signed distance functions. This allows us to robustly fuse information from sparse views and, at test time, to extrapolate beyond the observed poses or views. Moreover, we apply geometric constraints to co-learn the structure of the observed subject (including both body and clothing) and to regularize the radiance field to geometrical plausible solutions. Extensive experiments on multiple datasets demonstrate the robustness and accuracy of our approach and its generalization capabilities beyond the sparse training set of poses and views.

1 Introduction

Enabling free-viewpoint video of a human subject in motion is a challenging problem with many applications. Our work is motivated by the breadth of transformative 3D applications that would become possible, including immersive visualization of photos, virtual clothing and try-on modeling, fitness, or AR and VR for improved communication or collaboration. So far static scenes have been the primary subject of research. In pursuing realistic novel-view synthesis two schools of thought have been established: 1) 3D reconstruction methods aim to recover the geometry of the observed scene as accurately as possible before being displayed from novel views using classical rendering pipelines [30, 42]. 2) Image-based rendering techniques [7, 10, 40] and very recently neural radiance fields [29] primarily aim for image production quality without explicitly aiming at an accurate 3D geometric model. While these techniques sometimes explicitly or implicitly reconstruct the scene geometry as well, the geometry is not guaranteed to accurately resemble the true scene geometry. We argue that novel-view rendering and reconstruction are two sides of the same coin, and reliable viewpoint generalization, especially given relatively few input views, would require good quality for both. To this end, we propose a unified model in order to support robust both reconstruction and photo-realistic rendering. Dynamic scenes, especially those capturing a human in motion, add a new level of complexity to the problem: while static scenes can be observed from many views by a camera moving through the scene, any configuration of a dynamic scene is typically observed only from sparse views. Moreover, the scene geometry and its appearance may change drastically over time. To cope with the fewer views, some methods integrate scene knowledge over time by warping observations into a common reference frame [35, 37]. At test time, the information is warped back to the desired state and rendered from a novel view. Extrapolating to unseen motion, however, remains challenging. For scenes capturing people, this means that only poses seen during training can be rendered at test time. For some applications, however, rendering the subject under a large range of motions or in novel poses is desired. To make generalisation over poses and views possible, we rely on additional problem domain knowledge in the form of the human body model imGHUM [4]. imGHUM is an implicit signed distance function (SDF) conditioned on generative shape and pose

35th Conference on Neural Information Processing Systems (NeurIPS 2021), Sydney, Australia.

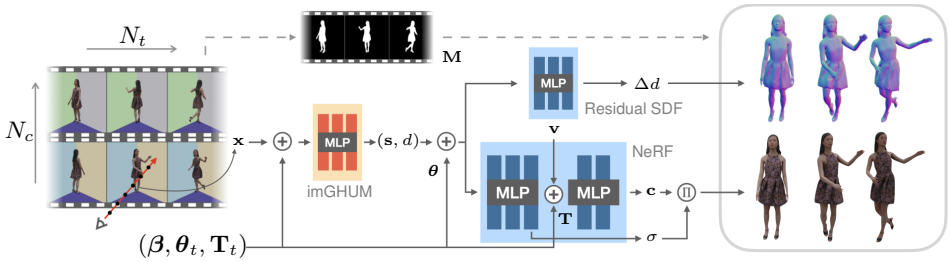

Figure 1: Overview of H-NeRF. Given a collection of images of a human performer collected from a sparse set of calibrated cameras, we train a geometry-aware neural radiance field by co-learning a deformable signed distance field. First, we estimate the body shape $\boldsymbol{\beta}$ and track the articulated pose $\boldsymbol{\theta}, \mathbf{T}$ using the implicit statistical human body model imGHUM (orange). imGHUM encodes all 3D spatial points $\mathbf{x}$ across frames with a 4D point descriptor $(\mathbf{s}, d)$ referencing a canonical frame. Using the foreground mask $\mathbf{M}$, we co-train a residual SDF and a NeRF network in that canonical space which integrate all visible 2D observations into a consistent implicit 3D geometry Δd and its view-depended $(\mathbf{v})$ radiance representation $(\mathbf{c}, \sigma)$. The trainable residual SDF and NeRF networks (in blue) are conditioned on the body pose $\boldsymbol{\theta}$ and the root transformation $\mathbf{T}$ to model pose-dependent geometric and appearance variations. Our framework supports both accurate 3D geometric reconstruction and free-viewpoint rendering, and generalizes well to novel views, shapes, and poses.

codes learned from a large corpus of dynamic human scans. In this work, imGHUM is used as the common reference frame for a neural radiance field and as a structured prior for robust reconstruction. Additionally, since imGHUM can represent a broad distribution of statistically valid human poses and shapes, we can render the reconstructed subject in novel poses and even with modified body shapes. In summary, our system supports photo-realistic free-view point rendering of a human subject as observed from sparse cameras. By conditioning on an implicit human body model, we can render novel body poses and shapes. Our carefully chosen losses ensure not only image quality but also plausible temporal reconstructions that can be used for the free-viewpoint visualisation of human performance capture.

2 Related Work

Human performance capture is the process of reconstructing the dynamic (4D) geometry of a human subject as observed in one or multiple synchronized views. Pioneering methods deform a rigged template mesh according to silhouettes observed in multiple views [6, 50], estimated skeleton key-points [12], or image correspondences [9]. Later systems relying on RGB-D video streams [5] or monocular capture [3, 2, 17, 52, 16, 15] have also been presented. All these methods rely either on a pre-scanned template mesh or on a body model that is deformed to fit the image evidence.

Neural representation for view synthesis. With the advent of neural networks researchers have begun to explore alternative solutions to represent a scene to support novel view synthesis and photo-realistic rendering; we refer the reader to [48] for a survey. Various forms of scene representation have been explored. Some methods use voxel grids to embed the scene [23, 45]. For rendering, the voxel grid is probed by shooting a ray and by linearly interpolating voxel values. These samples are then transformed into color values using a neural network. Other researchers have proposed neural textures [49, 43] that can be rendered with view-dependent effects or texture synthesis networks [22] for realistic rendering of meshes. In a similar spirit, other methods render point clouds, where each point carries local appearance information [26, 1]. Riegler and Koltun [40] reproject features from nearby views and rely on a SfM reconstruction scaffold for novel view synthesis. With the recent advent of implicit function networks [25, 34, 8, 27], such 3D representations have been explored for rendering and view synthesis with great success. In contrast to discrete voxel representations, textures, or point clouds, these methods represent the scene as a continuous function and thus are not bound to a specific image or volume resolution. In the pioneering work by Sitzmann et al. an implicit function produces features rendered using a neural renderer [46]. Follow up methods focus on 3D geometric reconstruction [44], and use 2D supervision [31, 53].

Neural Radiance Fields (NeRFs) are a recent approach to represent scenes for novel view synthesis. Mildenhall et al. [29] introduce Neural Radiance Fields as fully-connected neural networks representing a scene, whose input is a spatial query point and a viewing direction. The output is a volume

density and the emitted radiance at the query location in the direction of the viewer. By ray-tracing using this simple representation, one can generate photo-realistic images from novel views. Despite the excellent quality of results one drawback is the slow rendering time. To this end, researchers have presented faster versions that e.g. transform the radiance field into more efficient sparse grids [18] or remove the dependence on the view-direction during rendering by estimating a spherical harmonic representation of the radiance function [54]. Other derivatives improve fidelity or rendering time by tackling ambiguities in the original formulation [56], spatial decomposition into multiple NeRFs [39], or combining NeRF with sparse voxel fields [21]. Initial work adapting NeRF for dynamic scenes has been presented as well. Park et al. [35] produce "Nerfies" (NeRF-Selfies) from videos where subjects carefully move a camera around their head. The scene information is fused by warping query points into a canonical reference frame. Similarly, Pumarola et al. [37] produce dynamic NeRFs from synthetic animation data. Related to our approach, some methods integrate human body models to fuse information over time. A-NeRF [47] uses a skeleton to rigidly transform NeRF features to refine estimated 3D poses. A similar approach is followed in NARF [32] for view synthesis. Most related, Neural Body [36] attaches learnable features to the vertices of a SMPL body model [24]. These features are processed with a sparse 3D convolutional network, where the output forms a neural radiance field. In contrast to our approach, the resolution is bounded by the spatial resolution of the 3D conv net and no geometric supervision is performed. We highlight further differences in §5.

3 Background

Given a collection of images capturing a dynamic scene of a human in motion, seen from calibrated sparse camera views (in the limit a single monocular camera, as we will show), we aim to learn both the detailed temporal geometry of the human in motion, and enable rendering of the sequence from novel camera views and for novel human poses. To this end, our work unifies two main methodologies: 1) implicit 3D human representations and 2) volumetric radiance fields. In this section, we provide the relevant background on both representations, which we co-learn in a unified framework.

Neural Radiance Fields. A neural radiance field (NeRF) [29] represents a 3D scene as a continuous function of color volume densities. More specifically, the model consists of a neural network function F_ω that maps a 3D spatial point $\mathbf{x} \in \mathbf{R}^3$ and a viewing direction $\mathbf{v} \in \mathbf{R}^3$ to a volume density $\sigma \in \mathbf{R}^+$ and a radiance $\mathbf{c}(\mathbf{x}, \mathbf{v}) \in \mathbf{R}^3$ emitted towards the viewer. In practice, NeRF encodes the inputs $\mathbf{x}$ and $\mathbf{v}$ using a sinusoidal positional encoding $\boldsymbol{\gamma} : \mathbf{R}^3 \to \mathbf{R}^{3+6m}$ that projects a coordinate vector into a high-dimensional space using a set of sine and cosine functions of m increasing frequencies. Given a ray $\mathbf{r} = \mathbf{o} + s\mathbf{v}$ with N samples $\{\mathbf{x}\}$ originating from a camera location $\mathbf{o}$, NeRF integrates radiance values along the ray by means of alpha blending. The pixel/ray color is approximated with numerical quadrature [33]:

$$\mathbf{C}(\mathbf{r}) = \sum_{i=1}^{N} \alpha(\mathbf{x}_i) \prod_{j<i} (1 - \alpha(\mathbf{x}_j)) \mathbf{c}(\mathbf{x}_i, \mathbf{v}), \tag{1}$$

$$\alpha(\mathbf{x}_i) = 1 - \exp\big(-\sigma(\mathbf{x}_i)\delta_i\big), \tag{2}$$

where $\alpha(\mathbf{x}_i)$ is the transparency by accumulating transmittance along the ray, and $\delta_i = |\mathbf{x}_{i+1} - \mathbf{x}_i|$ is the distance between adjacent samples. The NeRF function F_w is fully differentiable and its network parameters w can be optimized using an image reconstruction loss [29]. An approximate 3D scene geometry $\mathbf{S}_F = \{\mathbf{x} | \sigma(\mathbf{x}) = \sigma_h\}$ can be extracted from the trained opacity field via Marching Cubes [20] at a density threshold σ_h.

Implicit Generative Human Models. Implicit human body surfaces are typically represented as the decision boundary of either binary occupancy classifiers [11, 41, 28] or signed distance functions [14, 4]. More specifically, our work builds upon the SOTA statistical implicit human model imGHUM [4] $H_\omega : (\mathbf{T}^{-1}\mathbf{x}, \boldsymbol{\beta}, \boldsymbol{\theta}) \to (d, \mathbf{s})$ that maps a 3D spatial point $\mathbf{x}$, unposed with root joint transformation $\mathbf{T} \in \mathbf{R}^{4\times3}$, to its signed distance value $d \in \mathbf{R}$ with respect to a body surface parameterized with body shape $\boldsymbol{\beta} \in \mathbf{R}^{16}$ and articulated pose $\boldsymbol{\theta} \in \mathbf{R}^{118}$. In addition to d, imGHUM returns implicit continuous semantics $\mathbf{s} \in \mathbf{R}^3$ of the query point which correspond the 3D coordinate of the nearest surface point defined on a canonical surface. We refer to the original paper [4] for details. Essentially, imGHUM builds a human-centric 4D semantic descriptor $(d, \mathbf{s})$ for all spatial points around the parameterized human body. imGHUM is trained from a large collection of human scans with diverse body shapes and poses, sharing the same generative shape and pose latent code with the mesh-based statistical human model GHUM [51]. The 3D implicit articulated human body $\mathbf{S}_H(\boldsymbol{\beta}, \boldsymbol{\theta}, \mathbf{T}) = \{\mathbf{x} | d(\mathbf{x}) = 0\}$ is defined by the the zero-isosurface of the signed distance field.

4 Method

In this section, we describe our main contribution H-NeRF, a novel neural network (fig. 1) that exploits both the power of volumetric radiance fields for learning complex scene structure and appearance, as well as implicit signed distance functions for accurate geometric reconstruction. Further, H-NeRF utilizes imGHUM, an implicit model of articulated human pose and shape, as a rich geometric prior, to integrate scene information over time, and to parameterize human articulation. Co-learning both a radiance field and a signed distance function of scene geometry consistently in a unified framework, enables 1) accurate 3D geometric reconstruction and volume rendering of a dynamic human on motion; 2) low demand on the number of training camera views; 3) consistent integration of 2D observations over time; and 4) good generalization capability to novel camera views, human shapes, and poses.

Given a sparse calibrated multi-view video of a human in motion, our task is to generate free-viewpoint video of the observed person and to reconstruct the underlying 4D geometry. We denote the input image collection with a resolution of $w \times h$ pixels as $\{\mathbf{I}_t^c \in \mathbf{R}^{w \times h \times 3} | c = 1, \ldots, N_c, t = 1, \ldots, N_t\}$, where c is the camera index, N_c is the number of cameras, t is the frame index, and N_t is the number of frames. For each image, we apply [13] to obtain the binary foreground human mask $\mathbf{M}_t^c \in \mathbf{R}^{w \times h}$. In addition, we obtain a temporal consistent imGHUM shape latent code $\boldsymbol{\beta}$ and pose codes $(\boldsymbol{\theta}_t, \mathbf{T}_t)$ at each frame index t by optimizing multi-view 2D keypoint and body segmentation losses [55]. We refer to our supplemental material for the detailed imGHUM fitting process.

In the sequel we first explain our adaptations to NeRF for the static case. imGHUM serves as a scene prior that helps to structure the observed scene and to learn more accurate geometry. We continue by explaining which additional changes are needed in the dynamic case. Hereby, imGHUM provides spatial correspondences across frames and is used as the common reference frame where we fuse information from different views and time instances.

4.1 Static Semantic Human NeRF

We first formulate H-NeRF for a human capture at a single moment in time ($N_t = 1$). From multi-view 2D observations, we co-learn a radiance field $F_\omega : \mathbf{x}, \mathbf{v} \rightarrow (\mathbf{c}, \sigma)$ for free-viewpoint rendering, and a signed distance function $\hat{H}_\omega : \mathbf{x} \rightarrow \hat{d}$ for 3D geometric reconstruction. We use $\hat{H}_\omega$ for the dressed subject to distinguish it from the minimally-dressed imGHUM body SDF H_ω.

Like NeRF, we formulate an L_1 image reconstruction loss to optimize F_w as

$$\mathcal{L}_{\text{rec}} = \sum_{\mathbf{r} \in \mathcal{R}} \|\bar{\mathbf{C}}(\mathbf{r}) - \mathbf{C}(\mathbf{r})\|_1, \tag{3}$$

where $\mathcal{R}$ denotes the batched set of all pixels/rays, and $\bar{\mathbf{C}}(\mathbf{r}), \mathbf{C}(\mathbf{r})$ are observed and rendered pixel color (cf. (1)), respectively. However, under sparse training camera views, the volumetric radiance field is not well regularized, leading to poor generalization to novel camera views, cf. fig. 2. Specifically, we observe that the model has difficulty in correctly representing the scene and separating the person from background. The model fails to learn a semantically meaningful opacity field, i.e. $\alpha = 0$ in the free space and 1 in the occupied space.

Coarse Scene Structuring. Using imGHUM fits for all training images, we can spatially locate the person in 3D space. We define a 3D bounding box $\mathbf{B} \in [\underline{\mathbf{S}_H} - \epsilon, \overline{\mathbf{S}_H} + \epsilon]$ around the detected person, where $\underline{\mathbf{S}_H}, \overline{\mathbf{S}_H}$ are the minimal and maximal coordinates of the human body surface $\mathbf{S}$ and ϵ is a spatial margin reserved for geometry not modeled by imGHUM. All radiance points that render the person should now reside inside the bounding box, leading to our 3D segmentation loss:

$$\tilde{\mathbf{C}}(\mathbf{r}) = \sum_{i=1}^{N} b(\mathbf{x}_i)\alpha(\mathbf{x}_i) \prod_{j<i} (1 - b(\mathbf{x}_j)\alpha(\mathbf{x}_j))\mathbf{c}(\mathbf{x}_i, \mathbf{v}), \tag{4}$$

$$\mathcal{L}_{\text{mask}} = \sum_{\mathbf{r} \in \mathcal{R}} \left\| \mathbf{M}(\mathbf{r}) \big(\bar{\mathbf{C}}(\mathbf{r}) - \tilde{\mathbf{C}}(\mathbf{r}) \big) \right\|_1, \tag{5}$$

where $b(\mathbf{x}_i)$ is 0 if outside of $\mathbf{B}$ and 1 otherwise, and $\mathbf{M}(\mathbf{r})$ is the image mask. We apply the mask here so the loss is only applied to structure that belongs to the subject and not to other scene geometry.

Unifying SDF with NeRF. After structuring the scene coarsely, we now couple the radiance field with implicit signed distance-based 3D reconstruction to further regularize the opacity distribution.

A signed distance function describing the detected person in the image naturally comes with a 3D classifier for all spatial points, where $\hat{d}(\mathbf{x}_i) > 0$ means $\mathbf{x}_i$ is in free space whereas $\mathbf{x}_i$ lies within the subject when $\hat{d}(\mathbf{x}_i) <= 0$. We rely on this observation to co-learn a SDF of the performer as an inductive bias for the radiance field. To this end, we introduce a pseudo alpha value $\dot{\alpha}(\mathbf{x}_i) = \phi(\gamma \hat{d}(\mathbf{x}_i))$ where ϕ is a Sigmoid activation function and γ controls the sharpness of the boundary. To refine the NeRF opacity semantics, especially for the volume around the human $\mathbf{B}$, we formulate two losses:

$$\hat{\mathbf{C}}(\mathbf{r}) = \sum_{i=1}^{N} \hat{\alpha}(\mathbf{x}_i) \prod_{j<i} (1 - \hat{\alpha}(\mathbf{x}_j)) \mathbf{c}(\mathbf{x}_i, \mathbf{v}), \quad \hat{\alpha}(\mathbf{x}_i) = b(\mathbf{x}_i)\dot{\alpha}(\mathbf{x}_i) + (1 - b(\mathbf{x}_i))\alpha(\mathbf{x}_i), \tag{6}$$

$$\mathcal{L}_{\text{blend}} = \sum_{\mathbf{r} \in \mathcal{R}} \big(\|\mathbf{M}(\mathbf{r})\big(\bar{\mathbf{C}}(\mathbf{r}) - \hat{\mathbf{C}}(\mathbf{r})\big)\|_1 + \eta \|(1 - \mathbf{M}(\mathbf{r}))\big(\bar{\mathbf{C}}(\mathbf{r}) - \hat{\mathbf{C}}(\mathbf{r})\big)\|_1 \big), \tag{7}$$

$$\mathcal{L}_{\text{geom}}(\mathbf{r}) = \sum_{i=1}^{N} b(\mathbf{x}_i) \text{BCE}\big(\phi\big(\lambda(\sigma_h - \sigma(\mathbf{x}_i))\big), \dot{\alpha}(\mathbf{x}_i)\big), \tag{8}$$

where $\hat{\mathbf{C}}(\mathbf{r})$ is the rendered pixel color with blended alpha values $\hat{\alpha}$ replacing NeRF alpha values α with SDF-based pseudo alpha $\dot{\alpha}$ for all ray points inside the bounding box $\mathbf{B}$. The first term in $\mathcal{L}_{\text{blend}}$ requires the rendered pixel color for all the intersecting rays within the human mask to come from the surface, whereas the second term assumes that all background color is formed from ray samples outside of $\mathbf{B}$. We set $\eta = 1$ when no other geometry than the person is inside $\mathbf{B}$ and tune η down if the assumption is violated (e.g. a person standing on a floor). The term $\mathcal{L}_{\text{geom}}$ uses the binary cross entropy loss to couple the NeRF surface boundary with the zero-isosurface of the signed distance function describing the subject. While the coupling terms given by (7) and (8) act as strong priors for the opacity distribution, during test time, we still rely on volumetric radiance rendering with learned NeRF alpha values α to support transparency effects and complex geometry such as hair.

Image-based SDF learning. Learning the signed distance field $\hat{H}_\omega$ from scratch using a sparse set of training images still remains challenging. The model often fails to reconstruct reasonable human geometry, even when using our coupling losses (7) and (8). We therefore leverage imGHUM as an inner layer for the target person and combine it with a light-weight residual SDF network $\Delta H_\omega : \mathbf{x} \rightarrow \Delta d$. The residual SDF models all surface details, including hair and clothing, that are not represented by imGHUM. The final signed distance for $\mathbf{x}_i$ becomes $\hat{d}(\mathbf{x}_i) = d(\mathbf{x}_i | \boldsymbol{\beta}, \boldsymbol{\theta}, \mathbf{T}) + \Delta d(\mathbf{x}_i)$. Given the training images, we learn the personalized residual SDF with our coupling losses, given by (7) and (8), and additionally apply geometric regularization:

$$\mathcal{L}_{\text{seg}} = \sum_{\mathbf{r} \in \mathcal{R}} \text{BCE}(\mathbf{M}(\mathbf{r}), \hat{d}_{\text{min}}(\mathbf{r})), \tag{9}$$

$$\mathcal{L}_{\text{eik}}(\mathbf{r}) = \sum_{i=1}^{N} b(\mathbf{x}_i)(\|\nabla_{\mathbf{x}_i} \hat{d}(\mathbf{x}_i)\|_2 - 1)^2, \quad \mathcal{L}_{\text{reg}} = \|\psi(\Delta d)\|_1, \tag{10}$$

where $\hat{d}_{\text{min}}(\mathbf{r})$ denotes the minimal signed distance for all sampled ray points and ψ is the ReLU activation function. The term $\mathcal{L}_{\text{seg}}$ ensures that if a pixel is inside the human segmentation mask, there should be at least one intersection between the ray and the 3D human surface and therefore $\hat{d}_{\text{min}}(\mathbf{r})$ should be non-positive. Otherwise, all ray samples should have positive signed distances. With $\mathcal{L}_{\text{eik}}$, we enforce the composite SDF $\hat{d}$ to be approximately a signed distance function, i.e. incorporating Eikonal regularization [14]. The term $\mathcal{L}_{\text{reg}}$ regularizes the residual distance Δd to be non-positive. This is because imGHUM should reside within the geometry and personalized geometric details given by Δd should be modeled on top of the skin surface.

4.2 Dynamic Semantic Human NeRF

We now extend the framework to model dynamic human motion. To implicitly model scenes where the human moves, we learn a consistent, continuous function $G_\omega : (\mathbf{c}, \alpha, \hat{d} | \mathbf{z}) \rightarrow (\mathbf{c}', \alpha', \hat{d}' | \mathbf{z}')$ for both the geometry and the appearance flow across frames. For generalization to novel poses or shapes, G_ω should be conditioned on a semantically meaningful latent code $\mathbf{z}$ that can be interpolated and should ideally have good extrapolation properties. To integrate scene information over time in a single radiance field, we follow the approaches in [35, 37] and warp observations into a canonical reference

frame. Given our constraints to G_ω, imGHUM, conditioned on its semantic shape and pose latent code $(\boldsymbol{\beta}, \boldsymbol{\theta}, \mathbf{T})$, naturally provides spatial correspondences across frames. Given two spatial points $\mathbf{x}$ and $\mathbf{x}'$ in the space of two human instances $(\boldsymbol{\beta}, \boldsymbol{\theta}, \mathbf{T})$ and $(\boldsymbol{\beta}', \boldsymbol{\theta}', \mathbf{T}')$ respectively, we decide that they are in correspondence if they have the same semantics and signed distances $(\mathbf{s}, d|\boldsymbol{\beta}, \boldsymbol{\theta}, \mathbf{T}) = (\mathbf{s}', d'|\boldsymbol{\beta}', \boldsymbol{\theta}', \mathbf{T}')$. Essentially, imGHUM assigns a 4D point descriptor $(\mathbf{s}, d) \in \mathbf{R}^4$ for any spatial point and deforms the volume continuously with respect to the parameterized articulated human body surface. Specifically, we apply $H_\omega : (\mathbf{T}^{-1}\mathbf{x}, \boldsymbol{\beta}, \boldsymbol{\theta}) \rightarrow (d, \mathbf{s})$ to map a spatial point $\mathbf{x}$ to a canonical point descriptor $(\mathbf{s}, d)$. We then modify the input to the NeRF function with the point descriptor as $F_w : (\mathbf{s}, d) \rightarrow (\mathbf{c}, \sigma)$, and similarly for the residual SDF function as $\Delta H_\omega : (\mathbf{s}, d) \rightarrow \Delta d$. imGHUM is pre-trained using a large corpus of 3D human scans, thus we keep it fixed in our network and directly use this prior to integrate structured geometric and appearance information across training frames. Given that the background scene is invariant to the human motion, we only apply the imGHUM warping function to spatial points inside the bounding box $\mathbf{B}$, which largely improves the computation time and memory consumption.

Pose-Dependent Geometry and Appearance. Training a single canonical NeRF and residual SDF from an image sequence integrates 2D observations into a consistent implicit geometric and volumetric radiance representation. However, we observe that fine level geometric and appearance variations caused by human motion are missing in the canonical NeRF and the residual SDF. To model such variations in geometry (clothing deformation and wrinkles) and in appearance (lighting and self-shadows), we condition the NeRF function F_ω, both the volume density σ (geometry) and color value $\mathbf{c}$ (appearance), as well as the residual SDF ΔH_ω (geometry), on the body pose code $\boldsymbol{\theta}$. In addition, we also notice that the relative position and rotation of the person with respect to the scene largely affects appearance (due to illumination effects), but should not affect the geometry. Based on this observation, we additionally condition the NeRF color on the person's root transformation as $\mathbf{c}(\mathbf{x}|\boldsymbol{\theta}, \mathbf{T})$.

H-NeRF Articulation. Differently from prior work [35, 37], all of our H-NeRF modules are now conditioned on the semantic human configuration latent code $(\boldsymbol{\beta}, \boldsymbol{\theta}, \mathbf{T})$, leading to an interpolatable SDF and radiance field. Moreover, due to imGHUM's capability to accurately model geometric volume deformation for diverse human poses and shapes, we have empowered H-NeRF with strong generalisation to novel poses and even body shapes. Concretely, during inference, one can simply set a different set of $(\boldsymbol{\beta}, \boldsymbol{\theta})$ to transfer the learned geometry and appearance to an unseen pose and shape configuration. For better generalization, we add Gaussian noise to the input code $(\boldsymbol{\theta}, \mathbf{T})$ during training, preventing the network to overfit to pose-dependent deformation and appearance effects seen during training. Similarly, we apply the same technique to NeRF conditioned on the view direction $\mathbf{v}$, when only a sparse set of training cameras is available.

Fine-tuning imGHUM Pose and Shape. We observe that the imGHUM fit can be a source of error when learning F_ω and ΔH_ω from dynamic image sequences. Instead of keeping them fixed, we further improve the fit during training by fine tuning a time-consistent shape correction $\Delta\boldsymbol{\beta}$ and per-frame pose correction $\Delta\boldsymbol{\theta}(t)$ with

$$\mathcal{L}_{\text{fit}} = \sum_{\mathbf{r}\in\mathcal{R}} \text{BCE}(\mathbf{M}(\mathbf{r}), d_{\text{min}}(\mathbf{r}|\boldsymbol{\beta} + \Delta\boldsymbol{\beta}, \boldsymbol{\theta} + \Delta\boldsymbol{\theta}(t))), \quad \mathcal{L}_{\text{inc}} = \|\Delta\boldsymbol{\beta}\|_2 + \frac{1}{N_t}\sum_{t=1}^{N_t} \|\Delta\boldsymbol{\theta}\|_2, \tag{11}$$

where $\mathcal{L}_{\text{fit}}$ aligns the imGHUM fit with the human foreground segmentation and $\mathcal{L}_{\text{inc}}$ regularizes the incremental corrections.

5 Experiments

In the following, we quantitatively and qualitatively evaluate H-NeRF through ablations and by comparing it with other methods. Please refer to our supplementary materials for more results and ablation experiments. We first detail our model architecture, the used datasets, and evaluation metrics.

Architecture and Training. We adapt the same network architecture for all of our experiments, where the trainable modules F_ω and ΔH_ω are composed of an eight 256-dimensional and six 128-dimensional MLP respectively, with a skip connection to the middle layer and with Swish activation [38]. As the original NeRF [29], we use 256 coarse and fine-level ray samples, for each of which we use 8- and 1-dimensional positional encoding for F_ω and ΔH_ω, respectively. We train the network using the Adam optimizer with a learning rate of 0.001 exponentially decayed by a factor

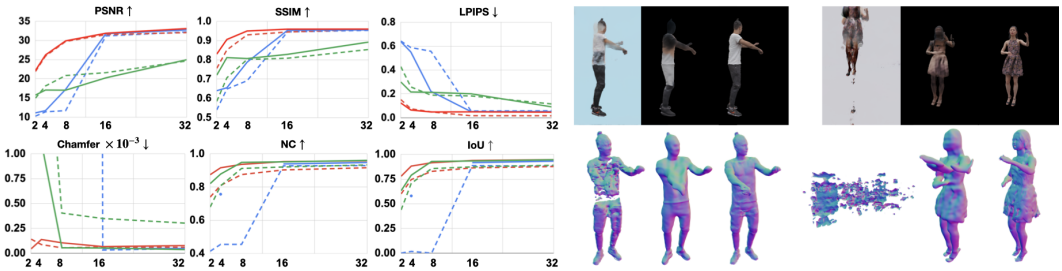

Figure 2: Left: H-NeRF (red, x-axis: #cameras) outperforms the original NeRF (blue) and IDR (green) in both novel view synthesis on 16 test cameras and 3D reconstruction of a static scene. NeRF and IDR fail under sparse camera views (solid line: RenderPeople scan; dashed line: GHS3D scan). Right: we qualitatively show novel views and reconstructed geometry for NeRF, IDR, and H-NeRF (from left to right) trained using four cameras.

Model	Dataset	PSNR ↑	SSIM ↑	LPIPS ↓	Ch $\times 10^{-3}$ ↓	NC ↑	IoU ↑
NeuralBody [36]	RenderPeople	27.33/23.52	0.888/0.827	**0.117**/0.247	0.536/0.63	0.908/0.892	0.864/0.824
	GHS3D	24.7	0.829	0.236	0.79	0.887	0.81
	PeopleSnapshot	24.62	0.849	0.160	–	–	–
	Human3.6M	24.86	0.82	0.189	–	–	–
H-NeRF (ours)	RenderPeople	**28.78/24.31**	**0.913/0.856**	0.125/**0.246**	**0.217/0.274**	**0.950/0.939**	**0.917/0.9**
	GHS3D	**24.92**	**0.852**	**0.232**	**0.218**	**0.932**	**0.89**
	PeopleSnapshot	**26.33**	**0.868**	**0.159**	–	–	–
	Human3.6M	**25.01**	**0.83**	**0.17**	–	–	–

Table 1: Quantitative evaluation of dynamic sequences on various datasets. When two metrics are reported they correspond to evaluation of training poses and novel poses at test cameras, respectively. PeopleSnapshot and Human3.6M are evaluated on novel poses under training views (with ground-truth images). Geometric metrics are only reported when ground-truth is available.

0.1 until the maximum number of iterations ($10k$ iteration of $4k$ ray batch size) is reached. We apply Gaussian noise with $\sigma = 0.1$ to the NeRF conditioning code $(\boldsymbol{\theta}, \mathbf{T}, \mathbf{v})$.

Dataset and Metrics. We provide both qualitative and quantitative evaluation on four different datasets: RenderPeople (8 sequences), GHS3D (14 sequences), PeopleSnapshot [3] (7 sequences) and Human3.6M [19] (5 sequences). The first two are synthetic datasets, rendering animated (RenderPeople) or 4D human scans (GHS3D) from four orthogonal cameras, where we have ground-truth geometry paired with images. We evaluate both image and 3D geometry reconstruction quality from two novel cameras, and qualitatively demonstrate the generalization capability to novel shapes and poses. The remaining datasets are real captured videos (PeopleSnapshot: monocular, Human3.6M: four cameras) without paired 3D geometry, where we only evaluate the rendered images. For image metrics, we adopt peak signal-to-noise ratio (PSNR ↑), structural similarity index (SSIM ↑) and learned perceptual image patch similarity (LPIPS ↓) [57]. For evaluation, we render the NeRF field inside the human bounding box $\mathbf{B}$ and compare to the ground-truth segmented image within a region of interest around the person. To evaluate geometric reconstruction quality, we report bi-directional Chamfer (Ch) L_2 distance, Normal Consistency (NC) and Volumetric Intersection over Union (IoU), evaluated on the mesh produced by Marching Cubes of the SDF with a resolution of 256^3.

Static Human Reconstruction under Sparse Cameras. H-NeRF learns a geometrically regularized volumetric radiance field unified with an imGHUM-based SDF, which significantly improves the robustness to sparse training camera views. In fig. 2, we reconstruct a static RenderPeople scan and a static GHS3D scan using the original NeRF [29], the state-of-the-art multi-view reconstruction approach IDR [53], and our H-NeRF with increasing number of cameras. Both, novel view image quality and geometry accuracy improve for all methods with increasing number of training camera images. However, in contrast to the competing methods, H-NeRF produces high quality output even under very sparse (2-8) training cameras, demonstrating the usefulness of our co-training approach.

Dynamic Human Reconstruction and Rendering. In the following, we evaluate H-NeRF's capabilities to reconstruct and render dynamic scenes (fig. 5). We compare H-NeRF against NeuralBody [36] (tab. 1), the current state-of-the-art for novel view synthesis of humans in motion. For fair comparison, we have trained NeuralBody with the same data as H-NeRF and use GHUM meshes (instead

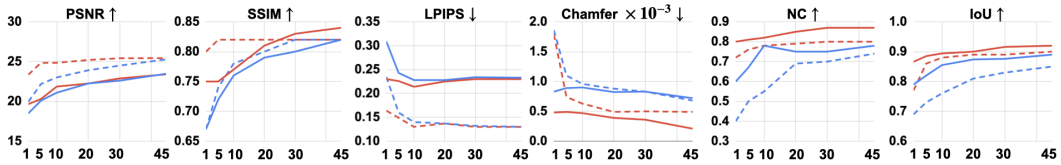

Figure 3: Frame Number Ablation. H-NeRF (red, x-axis: #training video frames) outperforms Neural Body (blue), evaluated on a RenderPeople (dashed) and a GHS3D (solid) sequence.

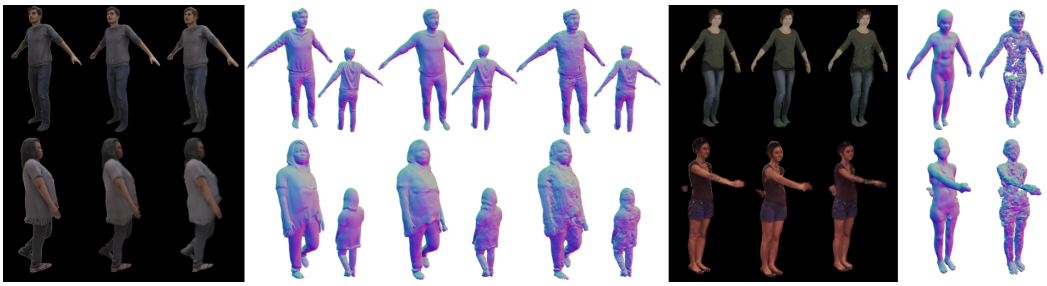

Figure 4: Qualitative results and comparisons with NeuralBody on the four different datasets. Left: GHS3D (top) and RenderPeople (bottom) ground-truth image, our result, NeuralBody, ground-truth geometry (front and back), our geometry, NeuralBody's geometry. Right: PeopleSnapshot (top) and Human3.6M (bottom) ground-truth image, our result, NeuralBody, our geometry, NeuralBody's geometry. Pay attention to the sharp renderings and the complete and detailed geometry produced by our method. Digital zoom-in recommended.

of SMPL) produced with the same pose and shape codes as used in our model for NeuralBody's structured latent codes. We further compare with Nerfies [35]. However, Nerfies has difficulties with the high degree of motion in our test sequences and fails for most of them. To this end, we consider the results as less meaningful and we report them only in the supplemental material for completeness.

H-NeRF is superior over NeuralBody across datasets and metrics, especially on geometry reconstruction. One possible explanation for NeuralBody's worse performance on view synthesis, is the fact that NeuralBody is not conditioned on the root transformation. Thus, global lighting effect are less well handled. Further, pose depended effects that go beyond body articulation are only implicitly modeled through relative distances of input mesh vertices. Finally, NeuralBody conditions on the frame index, which is set to zero for novel poses. On the PeopleSnapshot dataset where no view-depended and only subtle pose-depended effects are present, these limitations are not so apparent. In contrast, H-NeRF pays special attention to model both detailed geometry and appearance and is explicitly conditioned on pose and the root transformation for pose-depended geometry and appearance effects. This strategy pays off, especially in more complex scenarios.

Frame Number Ablation. We have now demonstrated H-NeRF's rendering and reconstruction capabilities for static and dynamic sequences. Next, we evaluate how many different poses or frames H-NeRF has to see during training for good pose extrapolation. We again compare against NeuralBody in this experiment. To this end, we have trained both methods with increasing number of frames uniformly distributed over the full sequence and compare the results in fig. 3. As expected, both methods perform better when trained with more data. However, H-NeRF performs overall better and more importantly, the quality degrades less for few frames, especially for geometry reconstruction. Our results demonstrate once more H-NeRF's robustness to little amounts of training data and its capability to reconstruct accurate geometry. To sum up, H-NeRF can be robustly trained with as little as 10 frames per camera (in a four camera set-up), resulting in a capturing effort of only minutes in practise.

Qualitative Results and Pose/Shape Extrapolation. Finally, we demonstrate H-NeRF's rendering and reconstruction accuracy also qualitatively (fig. 4). Consistent with the reported metrics, our synthesized novel poses appear sharper, more detailed, and contain less noise than current state-of-the-art. The estimated geometry is complete, smooth, and contains much of the detail present in the original scan, e.g. the clothing folds on the back of the person in the first row left. In contrast, geometries produced by NeuralBody are much more noisy and sometimes even incomplete. To

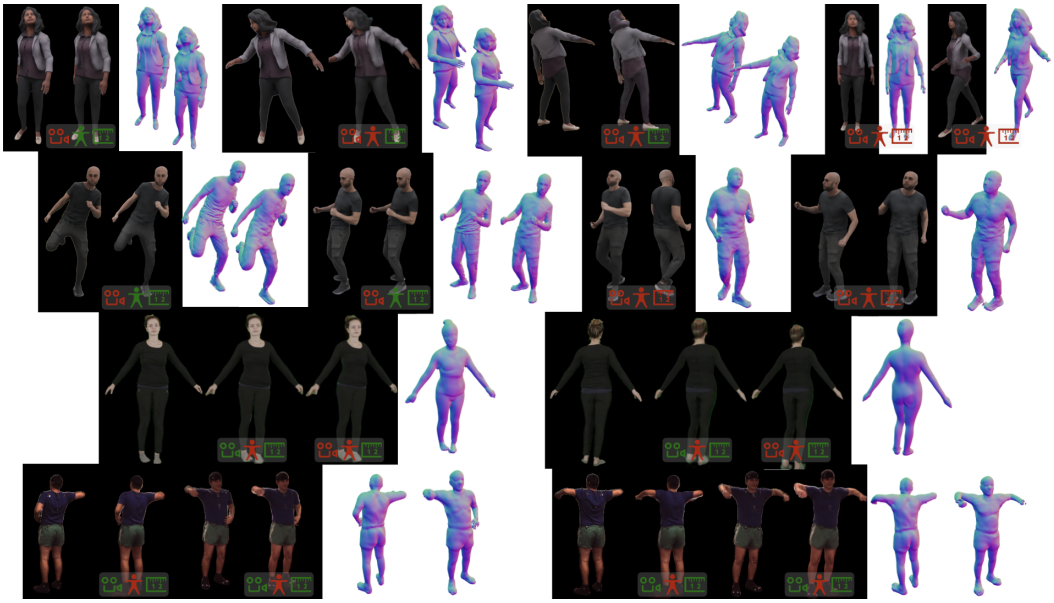

Figure 5: Qualitative results of H-NeRF on novel image synthesis. We show ground truth images and scans (left, if available) side-by-side with our results (right). Red icons correspond to test, green icons to training configuration. Symbols correspond to camera, pose, and shape, respectively. From top to bottom: RenderPeople, GHS3D, PeopleSnapshot and Human3.6M.

further demonstrate the versatility of our approach, we show examples of synthesized images and reconstructed geometry from novel viewpoints, in novel poses, and with altered body shape in fig. 5.

Limitations and Broader Impact. In the current setup, we assume full-body views of a single person in every-day clothing. Violating these assumptions, e.g. by placing another person in the scene would break the method although models of partial views or representation estimates of multiple people could be used towards more generality. Furthermore, our method has some sensitivity to the estimated body shapes and poses, as well as the quality of image segmentation. Although the process of learning to render could absorb certain inaccuracies, as pose, shape or segmentation are increasingly degraded, the method would fail eventually.

Our method paves the way towards novel immersive AR and VR applications. However, our approach is not targeted, or particularly useful for applications like visual surveillance or person identification as a particular set-up and a cooperating subject is needed. We do not build a audio-visual model that would be typical sought for deep fakes.

6 Conclusions

We have presented novel neural radiance field models for the photo-realistic rendering and the temporal reconstruction of humans in motion. Our objective is to extend the scope of the previous state of the art, focused on static scenes observed by a large number of cameras, by building dynamic models, which based on a very sparse set of views, can generalize well to novel camera views, human body poses, and even human body shapes. Our key contribution is in developing a new model with associated multiple losses, to specialize and constrain a generic NeRF formulation by using a compatible implicit statistical 3D human pose and shape model represented using signed distance functions. Our implicit geometric formulation captures not just the statistical human body form but also hair and clothing represented as an implicit residual network. Our model is trained end-to-end based on several novel losses and achieves very good results for both 3D reconstruction and rendering. Training the body model in an end-to-end rendering framework carries the promise to learn complex implicit skinning functions based on images only, a performance previously possible only in the realm of human capture using complex, laboratory placed, expensive 3D body scanners. We illustrate the favorable capabilities of our model by extensive experimentation using several datasets and against other state of the art techniques.

References

[1] Kara-Ali Aliev, Dmitry Ulyanov, and Victor Lempitsky. Neural point-based graphics. *arXiv preprint arXiv:1906.08240*.

[2] Thiemo Alldieck, Marcus Magnor, Bharat Lal Bhatnagar, Christian Theobalt, and Gerard Pons-Moll. Learning to reconstruct people in clothing from a single RGB camera. In *IEEE Conf. Comput. Vis. Pattern Recog.*, pages 1175–1186. IEEE, 2019.

[3] Thiemo Alldieck, Marcus Magnor, Weipeng Xu, Christian Theobalt, and Gerard Pons-Moll. Video based reconstruction of 3D people models. In *IEEE Conf. Comput. Vis. Pattern Recog.*, pages 8387–8397. IEEE, 2018.

[4] Thiemo Alldieck, Hongyi Xu, and Cristian Sminchisescu. imGHUM: Implicit generative models of 3D human shape and articulated pose. In *Int. Conf. Comput. Vis.*, 2021.

[5] Federica Bogo, Michael J. Black, Matthew Loper, and Javier Romero. Detailed full-body reconstructions of moving people from monocular RGB-D sequences. In *IEEE International Conference on Computer Vision*, pages 2300–2308. IEEE, 2015.

[6] Joel Carranza, Christian Theobalt, Marcus A Magnor, and Hans-Peter Seidel. Free-viewpoint video of human actors. *ACM Trans. Graph.*, 22(3):569–577, 2003.

[7] Shenchang Eric Chen and Lance Williams. View interpolation for image synthesis. In *Proceedings of the 20th annual conference on Computer graphics and interactive techniques*, pages 279–288, 1993.

[8] Zhiqin Chen and Hao Zhang. Learning implicit fields for generative shape modeling. In *IEEE Conf. Comput. Vis. Pattern Recog.*, pages 5939–5948, 2019.

[9] Edilson De Aguiar, Carsten Stoll, Christian Theobalt, Naveed Ahmed, Hans-Peter Seidel, and Sebastian Thrun. Performance capture from sparse multi-view video. In *ACM Trans. Graph.*, pages 1–10. 2008.

[10] Paul E Debevec, Camillo J Taylor, and Jitendra Malik. Modeling and rendering architecture from photographs: A hybrid geometry-and image-based approach. In *Proceedings of the 23rd annual conference on Computer graphics and interactive techniques*, pages 11–20, 1996.

[11] Boyang Deng, JP Lewis, Timothy Jeruzalski, Gerard Pons-Moll, Geoffrey Hinton, Mohammad Norouzi, and Andrea Tagliasacchi. Neural articulated shape approximation. In *Eur. Conf. Comput. Vis.* Springer, August 2020.

[12] Juergen Gall, Carsten Stoll, Edilson De Aguiar, Christian Theobalt, Bodo Rosenhahn, and Hans-Peter Seidel. Motion capture using joint skeleton tracking and surface estimation. In *IEEE Conf. Comput. Vis. Pattern Recog.*, pages 1746–1753. IEEE, 2009.

[13] Ke Gong, Xiaodan Liang, Yicheng Li, Yimin Chen, Ming Yang, and Liang Lin. Instance-level human parsing via part grouping network. In *Proceedings of the European Conference on Computer Vision (ECCV)*, pages 770–785, 2018.

[14] Amos Gropp, Lior Yariv, Niv Haim, Matan Atzmon, and Yaron Lipman. Implicit geometric regularization for learning shapes. In *Int. Conf. on Mach. Learn.*, pages 3569–3579. 2020.

[15] Marc Habermann, Lingjie Liu, Weipeng Xu, Michael Zollhoefer, Gerard Pons-Moll, and Christian Theobalt. Real-time deep dynamic characters. *ACM Trans. Graph.*, 40(4), aug 2021.

[16] Marc Habermann, Weipeng Xu, Michael Zollhoefer, Gerard Pons-Moll, and Christian Theobalt. Deepcap: Monocular human performance capture using weak supervision. In *IEEE Conf. Comput. Vis. Pattern Recog.* IEEE, jun 2020.

[17] Marc Habermann, Weipeng Xu, Michael Zollhöfer, Gerard Pons-Moll, and Christian Theobalt. Livecap: Real-time human performance capture from monocular video. *ACM Trans. Graph.*, 38(2):14:1–14:17, 2019.

[18] Peter Hedman, Pratul P Srinivasan, Ben Mildenhall, Jonathan T Barron, and Paul Debevec. Baking neural radiance fields for real-time view synthesis. In *Int. Conf. Comput. Vis.*, 2021.

[19] Catalin Ionescu, Dragos Papava, Vlad Olaru, and Cristian Sminchisescu. Human3.6M: Large scale datasets and predictive methods for 3d human sensing in natural environments. *IEEE Trans. Pattern Anal. Mach. Intell.*, 2014.

[20] Thomas Lewiner, Hélio Lopes, Antônio Wilson Vieira, and Geovan Tavares. Efficient implementation of marching cubes' cases with topological guarantees. *Journal of Graphics Tools*, 8(2):1–15, 2003.

[21] Lingjie Liu, Jiatao Gu, Kyaw Zaw Lin, Tat-Seng Chua, and Christian Theobalt. Neural sparse voxel fields. *NeurIPS*, 2020.

[22] Stephen Lombardi, Jason Saragih, Tomas Simon, and Yaser Sheikh. Deep appearance models for face rendering. *ACM Trans. Graph.*, 37(4):1–13, 2018.

[23] Stephen Lombardi, Tomas Simon, Jason Saragih, Gabriel Schwartz, Andreas Lehrmann, and Yaser Sheikh. Neural volumes: Learning dynamic renderable volumes from images. *ACM Trans. Graph.*, 38(4):65:1–65:14, July 2019.

[24] Matthew Loper, Naureen Mahmood, Javier Romero, Gerard Pons-Moll, and Michael J Black. SMPL: A skinned multi-person linear model. *ACM Trans. Graph.*, 34(6):248:1–248:16, 2015.

[25] Lars M. Mescheder, Michael Oechsle, Michael Niemeyer, Sebastian Nowozin, and Andreas Geiger. Occupancy networks: Learning 3d reconstruction in function space. In *IEEE Conf. Comput. Vis. Pattern Recog.*, pages 4460–4470, 2019.

[26] Moustafa Meshry, Dan B Goldman, Sameh Khamis, Hugues Hoppe, Rohit Pandey, Noah Snavely, and Ricardo Martin-Brualla. Neural rerendering in the wild. In *Proceedings of the IEEE/CVF Conference on Computer Vision and Pattern Recognition*, pages 6878–6887, 2019.

[27] Mateusz Michalkiewicz, Jhony K Pontes, Dominic Jack, Mahsa Baktashmotlagh, and Anders Eriksson. Deep level sets: Implicit surface representations for 3D shape inference. *arXiv preprint arXiv:1901.06802*, 2019.

[28] Marko Mihajlovic, Yan Zhang, Michael J. Black, and Siyu Tang. LEAP: Learning articulated occupancy of people. In *Proceedings IEEE/CVF Conf. on Computer Vision and Pattern Recognition (CVPR)*, June 2021.

[29] Ben Mildenhall, Pratul P. Srinivasan, Matthew Tancik, Jonathan T. Barron, Ravi Ramamoorthi, and Ren Ng. Nerf: Representing scenes as neural radiance fields for view synthesis. In *Eur. Conf. Comput. Vis.*, 2020.

[30] Roger Mohr, Long Quan, and Françoise Veillon. Relative 3d reconstruction using multiple uncalibrated images. *The International Journal of Robotics Research*, 14(6):619–632, 1995.

[31] Michael Niemeyer, Lars Mescheder, Michael Oechsle, and Andreas Geiger. Differentiable volumetric rendering: Learning implicit 3d representations without 3d supervision. In *IEEE Conf. Comput. Vis. Pattern Recog.*, June 2020.

[32] Atsuhiro Noguchi, Xiao Sun, Stephen Lin, and Tatsuya Harada. Neural articulated radiance field. In *Int. Conf. Comput. Vis.*, 2021.

[33] Michael Oechsle, Songyou Peng, and Andreas Geiger. Unisurf: Unifying neural implicit surfaces and radiance fields for multi-view reconstruction. In *Int. Conf. Comput. Vis.*, 2021.

[34] Jeong Joon Park, Peter Florence, Julian Straub, Richard A. Newcombe, and Steven Lovegrove. Deepsdf: Learning continuous signed distance functions for shape representation. In *IEEE Conf. Comput. Vis. Pattern Recog.*, pages 165–174, 2019.

[35] Keunhong Park, Utkarsh Sinha, Jonathan T. Barron, Sofien Bouaziz, Dan B Goldman, Steven M Seitz, and Ricardo Martin-Brualla. Nerfies: Deformable neural radiance fields. In *Int. Conf. Comput. Vis.*, 2021.

[36] Sida Peng, Yuanqing Zhang, Yinghao Xu, Qianqian Wang, Qing Shuai, Hujun Bao, and Xiaowei Zhou. Neural body: Implicit neural representations with structured latent codes for novel view synthesis of dynamic humans. In *IEEE Conf. Comput. Vis. Pattern Recog.*, 2021.

[37] Albert Pumarola, Enric Corona, Gerard Pons-Moll, and Francesc Moreno-Noguer. D-nerf: Neural radiance fields for dynamic scenes. In *IEEE Conf. Comput. Vis. Pattern Recog.* IEEE, jun 2021.

[38] Prajit Ramachandran, Barret Zoph, and Quoc V Le. Searching for activation functions. *arXiv preprint arXiv:1710.05941*, 2017.

[39] Daniel Rebain, Wei Jiang, Soroosh Yazdani, Ke Li, Kwang Moo Yi, and Andrea Tagliasacchi. Derf: Decomposed radiance fields. In *IEEE Conf. Comput. Vis. Pattern Recog.*, 2021.

[40] Gernot Riegler and Vladlen Koltun. Free view synthesis. In *European Conference on Computer Vision*, pages 623–640. Springer, 2020.

[41] Shunsuke Saito, Zeng Huang, Ryota Natsume, Shigeo Morishima, Angjoo Kanazawa, and Hao Li. Pifu: Pixel-aligned implicit function for high-resolution clothed human digitization. In *Int. Conf. Comput. Vis.*, pages 2304–2314, 2019.

[42] Johannes L Schonberger and Jan-Michael Frahm. Structure-from-motion revisited. In *Proceedings of the IEEE conference on computer vision and pattern recognition*, pages 4104–4113, 2016.

[43] Aliaksandra Shysheya, Egor Zakharov, Kara-Ali Aliev, Renat Bashirov, Egor Burkov, Karim Iskakov, Aleksei Ivakhnenko, Yury Malkov, Igor Pasechnik, Dmitry Ulyanov, et al. Textured neural avatars. In *IEEE Conf. Comput. Vis. Pattern Recog.*, pages 2387–2397, 2019.

[44] Vincent Sitzmann, Julien Martel, Alexander Bergman, David Lindell, and Gordon Wetzstein. Implicit neural representations with periodic activation functions. *Adv. Neural Inform. Process. Syst.*, 33, 2020.

[45] Vincent Sitzmann, Justus Thies, Felix Heide, Matthias Nießner, Gordon Wetzstein, and Michael Zollhöfer. Deepvoxels: Learning persistent 3d feature embeddings. In *Proc. Computer Vision and Pattern Recognition (CVPR), IEEE*, 2019.

[46] Vincent Sitzmann, Michael Zollhöfer, and Gordon Wetzstein. Scene representation networks: Continuous 3d-structure-aware neural scene representations. In *Adv. Neural Inform. Process. Syst.*, 2019.

[47] Shih-Yang Su, Frank Yu, Michael Zollhoefer, and Helge Rhodin. A-nerf: Surface-free human 3d pose refinement via neural rendering. In *Adv. Neural Inform. Process. Syst.*, 2021.

[48] Ayush Tewari, Ohad Fried, Justus Thies, Vincent Sitzmann, Stephen Lombardi, Kalyan Sunkavalli, Ricardo Martin-Brualla, Tomas Simon, Jason Saragih, Matthias Nießner, et al. State of the art on neural rendering. In *Comput. Graph. Forum*, volume 39, pages 701–727. Wiley Online Library, 2020.

[49] Justus Thies, Michael Zollhöfer, and Matthias Nießner. Deferred neural rendering: Image synthesis using neural textures. *ACM Transactions on Graphics (TOG)*, 38(4):1–12, 2019.

[50] Daniel Vlasic, Ilya Baran, Wojciech Matusik, and Jovan Popović. Articulated mesh animation from multi-view silhouettes. In *ACM Trans. Graph.*, pages 1–9. 2008.

[51] Hongyi Xu, Eduard Gabriel Bazavan, Andrei Zanfir, William T Freeman, Rahul Sukthankar, and Cristian Sminchisescu. GHUM & GHUML: Generative 3d human shape and articulated pose models. In *IEEE Conf. Comput. Vis. Pattern Recog.*, pages 6184–6193, 2021.

[52] Weipeng Xu, Avishek Chatterjee, Michael Zollhoefer, Helge Rhodin, Dushyant Mehta, Hans-Peter Seidel, and Christian Theobalt. Monoperfcap: Human performance capture from monocular video. *ACM Trans. Graph.*, 2018.

[53] Lior Yariv, Yoni Kasten, Dror Moran, Meirav Galun, Matan Atzmon, Basri Ronen, and Yaron Lipman. Multiview neural surface reconstruction by disentangling geometry and appearance. *Adv. Neural Inform. Process. Syst.*, 33, 2020.

[54] Alex Yu, Ruilong Li, Matthew Tancik, Hao Li, Ren Ng, and Angjoo Kanazawa. Plenoctrees for real-time rendering of neural radiance fields. In *Int. Conf. Comput. Vis.*, 2021.
[55] Mihai Zanfir, Elisabeta Oneata, Alin-Ionut Popa, Andrei Zanfir, and Cristian Sminchisescu. Human synthesis and scene compositing. In *AAAI*, pages 12749–12756, 2020.
[56] Kai Zhang, Gernot Riegler, Noah Snavely, and Vladlen Koltun. Nerf++: Analyzing and improving neural radiance fields. *arXiv preprint arXiv:2010.07492*, 2020.
[57] Richard Zhang, Phillip Isola, Alexei A Efros, Eli Shechtman, and Oliver Wang. The unreasonable effectiveness of deep features as a perceptual metric. In *CVPR*, 2018.